New Journal of Physics
The open access journal at the forefront of physics

Deutsche Physikalische Gesellschaft DPG IOP Institute of Physics

OPEN ACCESS

Orientation of biomolecular assemblies in a microfluidic jet

To cite this article: M Priebe *et al* 2010 *New J. Phys.* **12** 043056

New Journal of Physics
The open-access journal for physics

Orientation of biomolecular assemblies in a microfluidic jet

M Priebe[1], S Kalbfleisch[1], M Tolkiehn[1], S Köster[2], B Abel[3], R J Davies[4] and T Salditt[1,2,5]

[1] Institut für Röntgenphysik, Universität Göttingen, Göttingen, Germany
[2] Courant Research Centre Nano-Spectroscopy and X-Ray Imaging, Universität Göttingen, Göttingen, Germany
[3] Institut für Physikalische Chemie, Universität Göttingen, Göttingen, Germany
[4] ID13, ESRF, Grenoble, France
E-mail: tsalditt@gwdg.de

New Journal of Physics **12** (2010) 043056 (12pp)
Received 6 August 2009
Published 30 April 2010
Online at http://www.njp.org/
doi:10.1088/1367-2630/12/4/043056

Abstract. We have investigated multilamellar lipid assemblies in a microfluidic jet, operating at high shear rates of the order of $10^7\ s^{-1}$. Compared to classical Couette cells or rheometers, the shear rate was increased by at least 2–3 orders of magnitude, and the sample volume was scaled down correspondingly. At the same time, the jet is characterized by high extensional stress due to elongational flow. A focused synchrotron x-ray beam was used to measure the structure and orientation of the lipid assemblies in the jet. The diffraction patterns indicate conventional multilamellar phases, aligned with the membrane normals oriented along the velocity gradient of the jet. The results indicate that the setup may be well suited for coherent diffractive imaging of oriented biomolecular assemblies and macromolecules at the future x-ray free electron laser (XFEL) sources.

Contents

[5] Author to whom any correspondence should be addressed.

1. Introduction

Probing the structure and dynamics of large biomolecules and biomolecular assemblies in a hydrated and non-crystalline state poses a tremendous experimental challenge. The advent of highly brilliant pulsed x-ray radiation from free electron lasers (XFEL) has opened up a novel route to high-resolution imaging by short femtosecond (fs) pulses, possibly before radiation damage takes place [1, 2]. Based on these x-ray light sources, single cells, viruses, biomolecular complexes and possibly also single macromolecules may be imaged in a native, hydrated and unstained state. To this end, the samples can be delivered by a microfluidic system to the interaction volume with the x-ray beam [26]. The illuminated objects are then reconstructed from the oversampled coherent diffraction pattern by recently developed iterative algorithms [3]–[7]. Single-pulse coherent diffractive imaging (CDI) of a synthetic micrometer-sized test object on time scales shorter than the Coulomb explosion (i.e. the destruction of the sample following multiple ionization events) has already been demonstrated at a soft x-ray FEL [8]. Whether a single pulse of the upcoming instruments will be short and intense enough to achieve atomic or near atomic resolution remains a matter of debate. In any case, recovery of a full 3D structure would require multiple diffraction patterns of identical copies with different orientations, which have to be classified, aligned and phased numerically [2, 9].

Such experiments will require a spatially confined and windowless aqueous environment for biomolecular samples meeting the constraints of minimum background scatter and full compatibility with the x-ray beam propagating in ultrahigh vacuum. Moreover, the samples should be at least partially aligned uniaxially, in order to achieve efficient classification and alignment of different data sets before phasing, as has been quantified by computer simulation [9]. Alignment of small molecules by intense polarized laser beams [10, 11] has been discussed for single-molecule diffraction [12, 13]. For larger particles such as viruses, cells or biomolecular assemblies, alignment in microfluidic systems is a promising approach. Note that alignment can be achieved either by shear or by converging flow [27]. Here we show that a novel laminar microfluidic jet with diameters in the range of $D \in 10$–$50\,\mu$m and operating at shear rates in the range of $\dot{\gamma} \simeq 10^6$–$10^8\,\mathrm{s}^{-1}$ can be used for diffraction from partially oriented biomolecular assemblies even at current high-brilliance 3rd generation synchrotron sources. By placing the jet in the focus of a Kirkpatrick–Baez (KB) mirror system, we were able to measure the diffraction pattern of an oriented lamellar phase at sample volumes that are by several orders of magnitude smaller compared to previously used macroscopic Couette cells [14]–[18]. At the same time, the shear rates obtained are at least 2–3 orders of magnitude higher than in conventional instruments or in previously reported experiments on microfluidic devices operating at much smaller flow velocities [19]. Furthermore, the flow pattern in the jet is characterized by a high elongational (extensional) strain rate $\dot{\epsilon} = \partial v_z/\partial z \simeq 10^6\,\mathrm{s}^{-1}$ due to strong elongational flow along the nozzle axis z. The extraordinary high shear values are expected from simple models to be in the range where shear could induce denaturing of small globular proteins [20]. In this work, we do not find any indications of shear-induced structural changes in a lamellar lipid phase, aside from orientation. Importantly, the system fulfills the above requirements for future XFEL experiments, since the jet can be injected into vacuum due to its small diameter D [21]. The model lipid 1,2-dioleoyl-*sn*-glycero-3-phosphatidylcholine (DOPC) chosen here for a first experiment was motivated by the fact that it is in the fluid phase at room temperature and that its lamellar diffraction is both well known and of high signal-to-noise ratio.

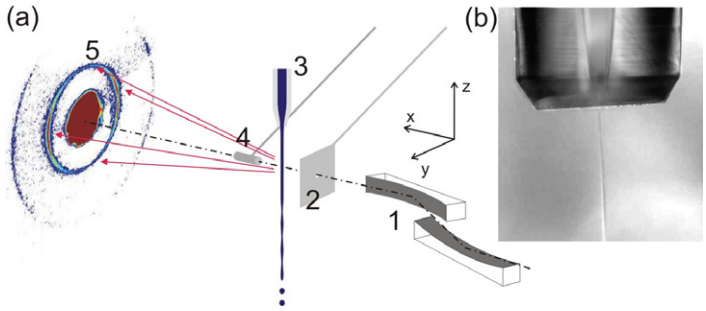

Figure 1. (a) Schematic of the experimental setup. The beam is (1) focused by an adaptive KB mirror system, (2) passes a pinhole–diode assembly to clean up the beam and to monitor the intensity, before it impinges onto the (3) microliquid jet, which can be scanned near the focal point in xyz. A small motorized beamstop (4) cuts the primary beam behind the sample, and the diffraction pattern is recorded by a CCD (5). In addition, a fluorescence detector and an optical microscope can be directed onto the jet. (b) Optical micrograph of the jet.

2. The setup and samples

The experiment has been carried out at the micro focus beamline $ID13$ of the European Synchrotron Radiation Facility (ESRF), Grenoble, using a photon energy of 12.437 keV set by a double Si(111) (Khozu, Japan) monochromator. An adaptive mirror KB system was then used to focus the beam down to $\simeq 5\,\mu$m with a flux of roughly 2×10^{10} photons/s (depending on the ring current and slit settings). In front of the focus, a 20 μm PtIr pinhole was used to clean up the beam. At the same time, the pinhole mount provided a miniaturized diode counter to monitor beam stability. The primary beam was absorbed by a 200 μm beamstop made of a Pb wire positioned a few cm behind the jet. An optical microscope (with a set of objectives, including an objective with $\times 50$ magnification and 0.5NA) could be moved into the setup for visual inspection of the jet, see figure 1. The jet was mounted on an xyz stage with sub-μm accuracy to scan the jet through the beam along the principal symmetry axes, parallel (z) and perpendicular (y) to the direction of flow, as well as to move it out for empty-beam measurements. The mechanical mount of the nozzle was designed to facilitate access to the jet from three sides, enabling (i) a large q-range, (ii) simultaneous recording of fluorescence (Vortex detector, SII NanoTechnology) and (iii) compatibility with the *in situ* optical microscope. The diffraction patterns were collected by a CCD detector (MarCCD 165) with a pixel size of 78.94 μm. A distance of $d_{\mathrm{det}} = 269.26$ mm behind the sample was determined from an Ag–Behenate calibration run and was then varied during the experiment as needed by relative translation from this reference position.

The nozzle (Microliquids GmbH, Göttingen, Germany) itself was made from quartz with an inlet diameter of ≈ 0.7 mm, which is narrowed by a conical shape function at the exit, to values of $D = 10$–$40\,\mu$m, respectively, as determined by optical microscopy. The high shear rates occur only as a short pulse corresponding to the transit times of the final $\Delta z \simeq 0.1$ mm at the nozzle tip, where the diameter is small. In contrast to a Couette cell, for example, the high shear rate acts only over a very short time span over which the flow is confined at the nozzle tip. We will call the corresponding shear rate profile the 'shear pulse', and its temporal width the 'shear transition time' τ_{s}. Averaged over all flow elements, the shear transition time can be

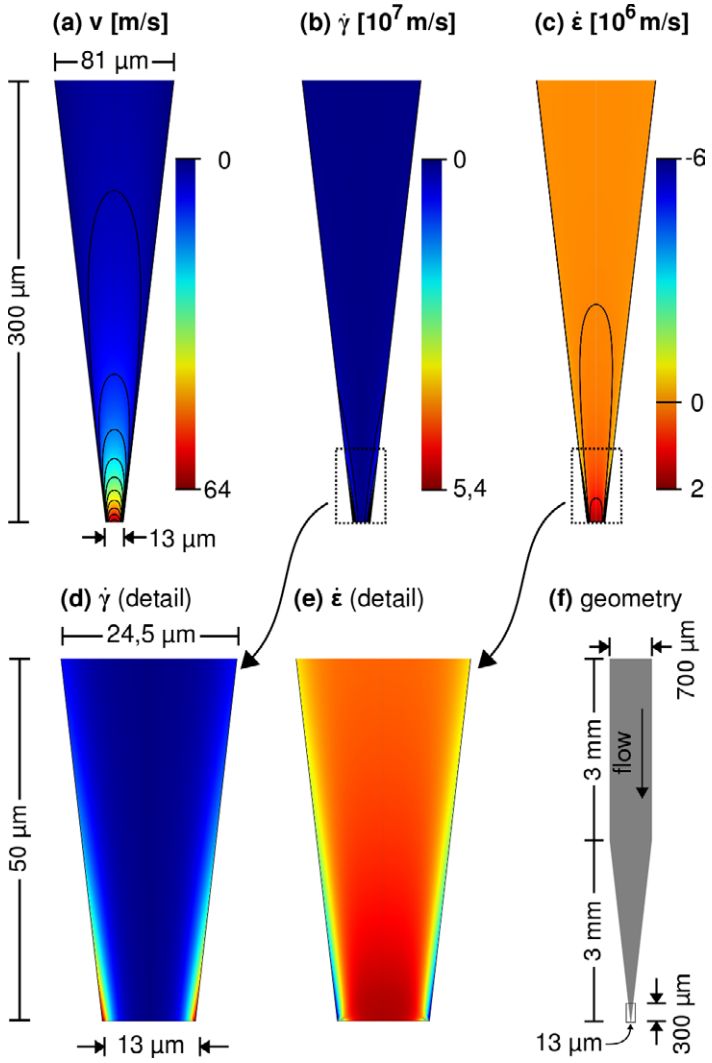

Figure 2. Finite element simulation (FEM) results (Comsol Multiphysics) of the flow profile at the nozzle tip, showing (a) the velocity field with the isolines of equal velocity and the spatial distribution of (b) shear rate $\dot{\gamma}$ and (c) elongational strain rate $\dot{\epsilon}$. The insets below show the lowest 50 μm at the nozzle tip of (d) $\dot{\gamma}$ and (e) $\dot{\epsilon}$. The entire geometry is sketched in (f), visualizing the rectangle corresponding to the simulation shown in (a)–(c). Note that the flow effects are dominated by the lowest part at the end of the nozzle. For the FEM simulation, the flow at the entrance is assumed to have constant velocity field, and a no-slip boundary condition is applied at the walls, while the flow is not restricted at the exit. While the shear rate is highest at the walls of the nozzle, the elongational strain rate is highest in the center and changes its sign toward the wall. In other words, the flow leads to a compression in the direct vicinity of the walls.

written as $\tau_s = \Delta z/\bar{v}$, where $\bar{v}$ is the average flow velocity at the tip. With $v = 10$–$10^2\,\mathrm{m\,s^{-1}}$, typical shear transition times are in the range $\tau_s = 1$–$10\,\mu$s. The velocity, shear and strain profiles as well as the elongational strain rate were calculated by the finite-element method (FEM) simulations (Comsol Multiphysics), see figure 2, for the measured tip geometry with an

opening angle $\alpha \approx 13^\circ$ and the viscosity of the lipid solution $\eta = 3.24 \times 10^{-3}$ Pa s, as measured by an Ubbelohde viscometer (Schott Instruments GmbH). Note that the viscosity tensor for smectic liquid crystals generally has three independent coefficients [22]. Only an orientationally averaged (effective) macroscopic bulk viscosity is considered here. The flow simulations are also carried out for an isotropic Newtonian fluid and should only serve for comparison with an idealized case, in particular since the more general situation of a liquid crystalline suspension cannot easily be treated. The liquid is supplied by a standard PC-controlled HPLC pump (Jasco) with flow rates ranging from 0.2 to 1 ml min^{-1}, and pressures up to 120 bar. The sample suspension (25 ml) is stored in a reservoir from which the HPLC pump is fed, using HPLC capillaries made from polyetheretherketone (PEEK). Two inline filters are used in front of the nozzle. The solution is recollected below the free jet and fed back to the reservoir in a closed loop arrangement. This operation mode provides a stable jet for several hours. No degradation of the sample suspension was observed, e.g. as judged from eventual changes in the diffraction pattern.

The lipid 1,2-dioleoyl-*sn*-glycero-3-phosphatidylcholine (DOPC) supplied by Avanti Polar Lipids (Alabaster, AL) was suspended in ultrapure water (Milli-Q) at a concentration $c = 100$ mg ml^{-1}, yielding self-assembled multilamellar vesicles (MLVs). In the following, the MLVs can be considered as the multilamellar membrane domains of the suspensions, not necessarily of spherical shape. The sample concentration was chosen to be in a range where the membranes are fully hydrated coexisting with excess water. At the same time, the scattering signal was still quite intense. How the excess water and lipid domains are distributed is difficult to assess. Even in the equilibrium state (in the absence of flow), it is hard to quantify domain sizes and the mesoscopic structure of the suspension, since no single length scale appears, e.g. in polarization microscopy. At the same time, the measured d-spacing and overall shape of the diffraction pattern obtained in the jet did not give any indications of phase separation, and aside from the orientation the diffraction patterns did not differ from those obtained in capillaries. We note that the simplified description of this complex fluid in terms of Newtonian flow which we use below is characterized by a single scalar (isotropic) viscosity. Of course, anisotropy of smectic liquid crystalline phases, phase separation in the shear flow, as well as viscoelastic effects cannot be described in this framework. In addition to the MLV suspension, small unilamellar vesicles (SUV) were prepared by dissolving DOPC at $c = 1$ mg ml^{-1} in Hepes buffer prepared with ultrapure water, and sonication to clarity (Sonoplus, Germany).

Finally, let us close the section by briefly considering the shear profile. Let $R(z)$ denote the radius of the conical nozzle that is tapered along z, and $\dot{V}$ the flow rate. For Poiseuille flow we would get $\dot{\gamma}(r) = (4/\pi)(\dot{V}/R^3)(r/R)$, with $r = \sqrt{x^2 + y^2}$. Averaged over the lateral cross section $\pi R(z)^2$ of the nozzle, the shear rate $\langle \dot{\gamma}(z) \rangle_{xy} = (8/3\pi)(\dot{V}/R(z)^3)$ increases strongly toward the tip of the nozzle. The vertical length Δz over which $\langle \dot{\gamma}(z) \rangle_{xy}$ peaks, where $\langle \cdots \rangle_{xy}$ denotes the average in the xy-plane, then scales with the radius of the nozzle at the tip $R(z = 0)$. The smaller the tip radius R, the more localized the maximum shear $\dot{\gamma}_{\max}$. The FEM simulation shows a velocity profile that matches $v(r) \propto (1 - (r/R)^\alpha)$ with an exponent $2 \leqslant \alpha \leqslant 8$ increasing toward the nozzle exit and thus deviates from the simple Poiseuille flow. However, the basic scaling relations $\langle \dot{\gamma}(z) \rangle \propto (\dot{V}/R(z)^3)$, and $\Delta z \propto R$ are maintained. Downstream from the nozzle exit, the flow has not been simulated, but a transition to plug flow is expected over length scales of a few D [23].

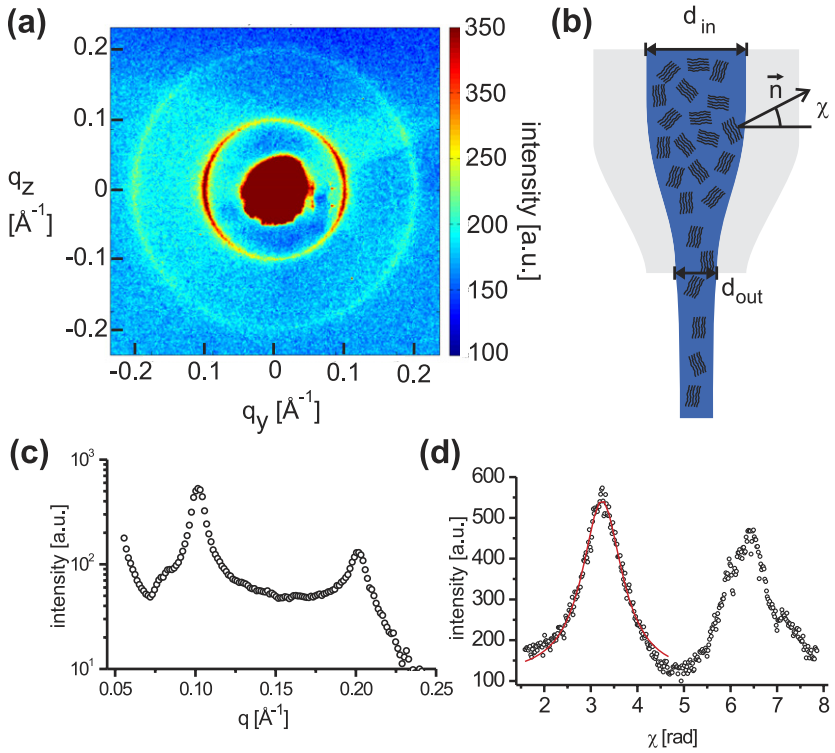

Figure 3. (a) Typical diffraction pattern (raw data) of a multilamellar sample with the circular segments of the $n = 1$ and $n = 2$ lamellar orders, recorded by the CCD. (b) Schematic of the shear-induced orientation of lamellar domains. (c) The radial intensity profile derived from (a), showing two lamellar reflections. (d) The azimuthal distribution fitted to a Lorentzian with a linear background (solid line).

3. Results

Figure 3(a) shows a typical diffraction pattern of a partially oriented multilamellar phase with the characteristic circular segments of the first $n = 1$ and second $n = 2$ lamellar orders. The lamellar diffraction is stronger in the horizontal plane than in the vertical, indicating an orientational distribution of the lamellae normal vectors $\vec{n}$, which peaks in the horizontal plane. A corresponding schematic of lamellar domains with partial alignment in the flow at the nozzle tip is presented in figure 3(b). Figure 3(c) shows the intensity profile averaged over the azimuthal angle χ for the same data as those shown in (a), as a function of radial momentum transfer $q = \sqrt{q_x^2 + q_y^2}$. The peak position $q_{n=1}$, intensity and width of the first lamellar order are then determined by least-square fitting. The $n = 1$ maximum at $q_{n=1} \approx 0.10\,\text{Å}^{-1}$ indicates a lamellar spacing of $d = 62.3$ Å. This d-spacing was found to be constant as a function of $\dot{\gamma}$ and the exact position in the jet, to within 0.4 Å. Next, an interval around the peak is determined and used to integrate over the peak along the radial direction. The (radially) integrated intensity or the $n = 1$ peak can then be plotted against azimuthal angle χ, see figure 3(d), reflecting the angular distribution function of the membrane normal vectors. Finally, the width ω (full-width at half-maximum (FWHM)) of the distribution function is obtained from a least-square

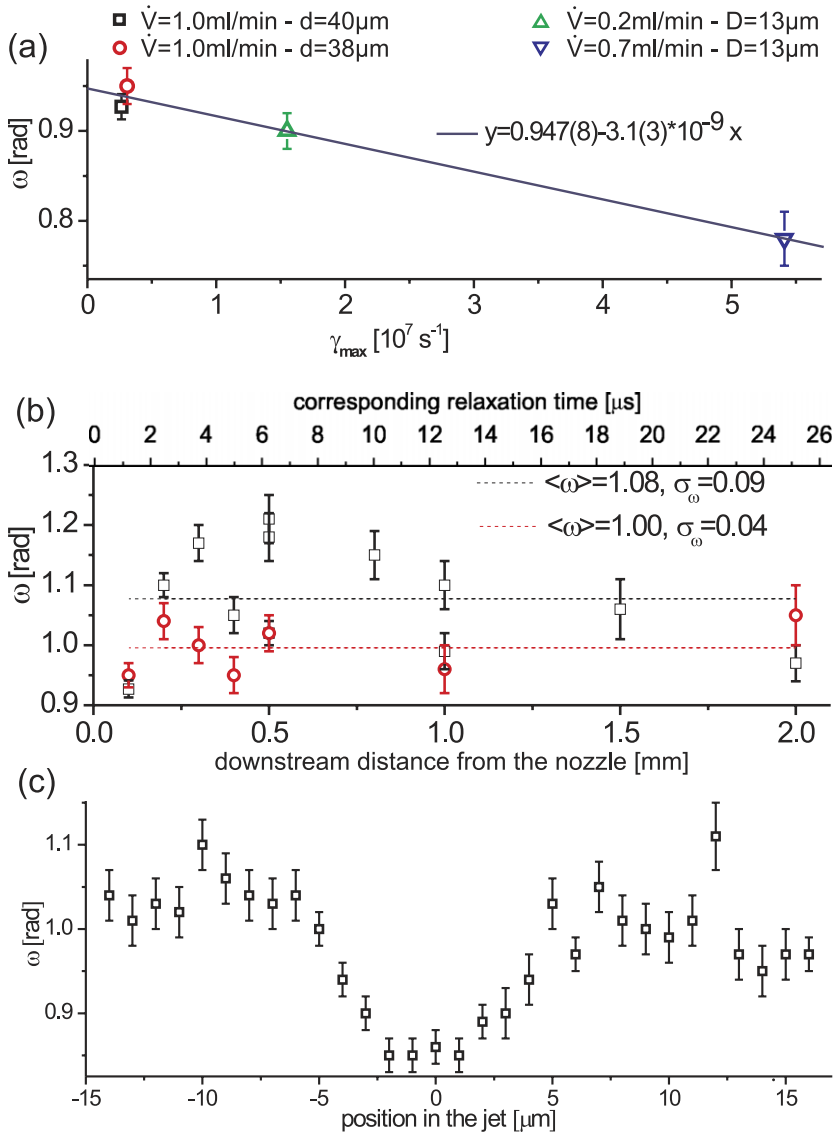

Figure 4. (a) Values of ω for different flow rates and nozzle diameters D, each measured 0.1 mm downstream from the nozzle exit and plotted against the maximum shear rate at the nozzle exit $\dot{\gamma}_{\max}$, along with an empirical linear fit (solid line). In (b), the mosaicity ω (FWHM of the fitted Lorentzian) is plotted against the downstream distance z from the nozzle and the corresponding transition time after passing the nozzle exit. (c) Plot of ω as a function of distance from the center of the jet $\omega(y)$.

fit of the χ-dependent distribution to a Lorentzian with a linear background. This width of the orientational distribution function is also called mosaicity ω.

The following dependences were investigated: (i) the orientation as a function of shear rate $\omega(\dot{\gamma})$ from variation of flow rate $\dot{V}$ and nozzle diameter D, (ii) lateral profile $\omega(y)$ from scanning the jet through the beam in the focal plane and (iii) vertical profile $\omega(z)$ from z-scans, respectively. Figure 4(a) shows the variation of the angular width ω as a function of maximum

shear rate $\dot{\gamma}_{\max} = 4\dot{V}/(\pi R^3)$, calculated for Poiseuille flow with a flow rate $\dot{V}$ and a nozzle radius $R = D/2$. While D is measured by optical microscopy, $\dot{V}$ is a control parameter of the HPLC pump. The lamellar alignment persists even downstream (below) from the nozzle exit, where a transition from Poiseuille to plug flow can be expected, as evidenced by scanning the beam along z parallel to the jet downstream from the nozzle. The corresponding mosaicity values $\omega(z)$ are shown in figure 4(b) for two different runs with control parameters $D \simeq 40\,\mu$m and $\dot{V} = 1\,\text{ml}\,\text{min}^{-1}$, as detailed in the legend. The values were obtained from scans in defocus to increase the beam size on the jet, resulting in an average over y. Note that a larger beam size was in some instances also helpful for avoiding misalignment if the jet was not exactly vertical. As can be seen, the orientational distribution does not change significantly along the z-axis for the $D \simeq 40\,\mu$m data, while there is a slight increase for the smaller jets $D = 13\,\mu$m (not shown). In other words, once that partial alignment is obtained from the shear, there is little or incomplete relaxation over the accessible time scales $\tau_j \simeq 2$–$25\,\mu$s (depending on average velocity and decay length), which the lamellar phase spends in the liquid filament before breakup into droplets. Experimentally, τ_j is given by the decay length as observed in the online microscope, and by the average velocity calculated from the flow rate and jet diameter. Finally, figure 4(c) shows the dependence $\omega(y)$ as the jet is scanned perpendicular to the jet along y at $D = 40\,\mu$m and $\dot{V} = 1\,\text{ml}\,\text{min}^{-1}$, while x is adjusted to the focal plane, and $z = 0.1$, below the nozzle. For a Poiseuille flow profile and the corresponding linear increase in the shear rate $\dot{\gamma}$ for increasing $|y|$, the smallest ω would be expected at the sides of the jet, in contrast to the experimental results, which show a pronounced dip at the center and a flat profile at higher radii. The variation in the middle is particularly remarkable, as neither the diameter of the jet along the optical axis nor the average shear profile for Poiseuille flow varies significantly in this range. This behavior may be an indication that alignment by elongational strain may play a leading role at the center of the jet, as discussed in the next section.

By scanning the liquid jet in the y-direction through the focus of the x-ray beam, we have also observed strong horizontal reflection, when the x-ray beam impinges tangentially on the jet interfaces on either side. This effect was observed for samples with and without lipid and leads to elongated streaks of radiation on the detector in the horizontal direction, as illustrated in figures 5(a) and (b) for the case of a $D = 38\,\mu$m jet, operating at $\dot{V} = 1\,\text{ml}\,\text{min}^{-1}$ with a suspension of SUVs (SUVs preparation). The intensity decay in the streak was analyzed by a free fit to an algebraic decay $I \propto q_y^{-\beta}$, yielding an exponent of $\beta = 3.4 \pm 0.2$, see figure 5(c). This value is lower than the usual $\beta = 4$ for planar interfaces, and could possibly be understood by a generalization of Fresnel reflectivity for curved interfaces. If this can be accomplished, details of the surface profile, i.e. by absorption of lipid molecules, and of the roughness may become accessible in future. In addition, interface corrugations and fluctuations preceding the decay of the jet in droplets can be expected to change the vertical and horizontal lineshapes of this streak.

4. Discussion and conclusion

The experimental results are found to be highly reproducible for all the samples tested, and the extracted values for the mosaicity do not depend critically on the detailed procedures, e.g. selecting the integration parameters, background subtraction, or parameters of the fitting algorithms. Data accumulation time and signal-to-noise ratio values are equally very satisfactory

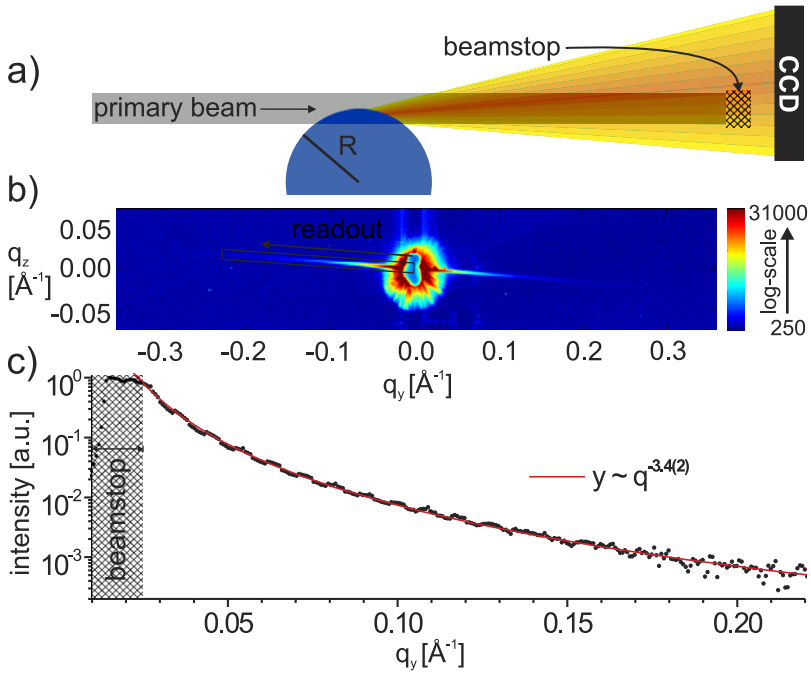

Figure 5. (a) Scattering geometry with the x-ray beam impinging on the jet surface tangentially. After traversing the jet, the transmitted beam is absorbed in the beamstop, while a part of the beam is reflected over a range of incidence angles corresponding to the illuminated sector of the jet. Reflection occurs for both directions in the form of a characteristic streak pattern visible on the CCD detector (b). In the particular case, data were recorded at $z = 0.5$ mm downstream from the nozzle. The jet was exiting the nozzle at an oblique angle, giving rise to the slightly tilted streaks. The contour of the slice used for further analysis is also indicated. The vertically integrated intensity in the slice is plotted against the horizontal q_y axis, see (c). The intensity decay (solid circles) was fitted to an algebraic decay (solid line), see text.

and prove that the setup is well suited for the purpose of diffraction and diffractive imaging studies of biomolecular assemblies and biomolecules.

Let us first discuss the mechanisms of lamellar alignment. The maximum shear rate $\dot{\gamma}_{\max}$ is by two to three orders of magnitude higher than the typical literature values obtained in standard macroscopic Couette cells, used extensively for complex fluid experiments. At the same time, the orientation ω, which can also be rephrased in terms of an orientational order parameter $S = (3\langle\cos^2\chi\rangle - 1)/2$, is quite comparable to the values reported for shear-induced alignment in lamellar phases. The measured mosaicities $\omega \in \{0.7..1.3\}$ rad are probably much higher than what can reasonably be assumed for the high shear rate, if the shear rate was applied in steady state. In contrast to classical Couette cells, where only the shear rate determines the alignment of lamellar domains in the flow, here both shear rate $\dot{\gamma}$ and elongational strain rate $\dot{\epsilon}$ are important for the observed alignment properties. The fact that ω is smallest in the center of the jet indicates that alignment by elongational strain plays an important role. While the shear rate is highest at the walls of the nozzle, the elongational strain rate is highest at the center and changes its sign

toward the wall. In other words, the flow leads to a compression at the rim. Therefore, the two effects of shear and elongational strain may act in opposite senses in the outer regions near the walls (at the rim) of the conical nozzle. This may explain the difference in ω of about 0.1 rad that was observed in the scans, where the x-ray beam was scanned across the jet. From FEM simulations we find $\dot{\epsilon} < \dot{\gamma}$ for all the flow parameters tested, see figure 2. On the other hand, the elongational strain rate is rather uniform at the center of the nozzle as a function of the radius and peaks at about $\simeq 2 \times 10^6\,\mathrm{s}^{-1}$ at the nozzle exit. To what extent the shear rate and the elongational strain rate each determine the multilamellar distribution function of the lamellar domains at different positions in the jet cannot be determined from the oversimplified FEM simulations. Nevertheless, experimental evidence is strong that both effects play important roles. For each of the effects, the Weissenberg number Wi would predict full (saturated) alignment of the lamellae, in contrast to the partial alignment with the rather broad distribution function observed.

Next, let us consider the time scales of the experiment, in order to explain the partial alignment. The relatively high value of ω (low shear alignment) could be explained by considering the short duration of high shear rate in the shear pulse, and in an equivalent manner the short duration of the elongational strain rate. In the following, we will phrase the argument in terms of 'shear pulse', but it may apply in an analogous sense to the 'elongational strain pulse'. We will distinguish three characteristic time scales: τ_s for the duration over which the maximum shear is applied, i.e. the transition time of a fluid volume element in the nozzle tip, τ_j for the transition time in the free jet before decay into droplets and finally τ_o for the time scale over which orientation of a lamellar domain takes place. While most of the literature experiments were carried out in stationary non-equilibrium conditions of shear, the present experiment deals with a short pulse of shear, meaning that the high shear rate is applied only over a very short time span that the fluid traverses the small diameter nozzle tip. The duration of this 'shear pulse' can be estimated from $\tau_\mathrm{s} = \Delta z/\bar{v}$, where $\bar{v} = \dot{V}/(\pi R^2)$ is the average flow velocity at the nozzle exit (tip). Using the simplified scaling arguments given above, the integral shear shows no or little variation with respect to the control parameters $\dot{V}$ and R, as $\int \dot{\gamma}\,\mathrm{d}t \simeq \dot{\gamma}_\mathrm{max}\tau_\mathrm{s} \propto (\dot{V}/R^3)(\Delta z/\bar{v}) \simeq \mathrm{const}(R, \dot{V})$. Therefore, the weak dependence on $\omega(\dot{\gamma})$ observed in the experiment becomes plausible. If $\dot{\gamma}$ increases, τ_s decreases. If the resulting alignment is a linear response to the integral shear rate and the alignment order parameter S is small, a proportional response $S \propto \dot{\gamma}\tau_\mathrm{s}/\tau_\mathrm{o}$ is a reasonable assumption. This would also be in good agreement with the observation that the lamellar ordering remains oriented along the jet, since the experimental results indicate that $\tau_\mathrm{s} \lesssim \tau_\mathrm{j} < \tau_\mathrm{o}$.

Which typical time scales τ_o for re-orientation of a multilamellar lipid mesophase can be expected, if the shear (or elongational strain) is turned on or relaxed? Let us assume that the time scale to reorient a domain of size L is linked to the typical time scale of an undulation mode of the corresponding wavelength. Undulation modes in lamellar phases decay with relaxation rates $\tau^{-1}(q_{||}) = \kappa/(\eta_3 d)q_{||}^2$, while fluctuations of a free bilayer decay with $\tau^{-1} \propto q_{||}^3$ [24], where κ is the bending stiffness and η_3 is the sliding viscosity. For realistic values of $\kappa = 15k_\mathrm{B}T$ and $\eta_3 = 0.016\,\mathrm{Pa\,s}$ [25], $\tau_\mathrm{o} > \tau_\mathrm{j}$ would hold, for reasonable domain sizes of $L \geqslant 1\,\mu\mathrm{m}$. Smaller length scales would be unreasonable to assume for domain sizes in multi-lamellar phases and would not match the patterns observed in polarization microscopy. At the same time, the Weissenberg number, which can be estimated here to be of the order of $Wi = \dot{\gamma}\tau_\mathrm{o} \simeq 10^7 \times 10^{-2} = 10^5$, indicates perfect alignment if the shear were stationary.

Thus, it turned out in the course of the study that the long time scales associated with reorientation of large lamellar domains in multi-lamellar systems prevent a complete reorientation of the domains during the nozzle flow. As a consequence, the dependences on the flow parameters are rather small. If, on the other hand, systems with much smaller relaxation times could be measured, a transition from isotropic to high orientation could possibly be triggered by the flow parameters. However, we doubt that such systems could be multilamellar lipid phases, since the collective dynamics of the undulations always extend to very long time scales for small spatial Fourier components. Aggregates with less pronounced dispersion rates or non-aggregated biomolecules, however, may fall under this category, but will be considerably more challenging in terms of signal-to-noise ratio, at least at present sources. For small unilamellar vesicles (SUV) shorter relaxation times can also be expected, but the action of the shear and elongational strain is less clear. The parameters of the current experiment did not allow for enough scattering signal in the case of the SUV samples, so that no conclusions can be drawn on this issue.

Finally, in view of future extension of this work, we briefly consider orientation of solvated macromolecules rather of assemblies or aggregates. Taking the Zimm time for macromolecules of radius of gyration $R_g \geqslant 8\,\mathrm{nm}$, we get $Wi = \dot{\gamma}\tau_o \simeq 10^7 \times \eta R_g^3/(k_B T) > 1$, and hence can expect shear alignment of the chain in the stationary state. At the same time, $\tau_s \gg \tau_o$ assures that this state is reached in the nozzle. Corresponding experiments are planned and probably feasible at 3rd generation synchrotron sources, but are more demanding in terms of flux than what has been described here. Finally, the microliquid setup presented here should enable the delivery of oriented biomolecules for single-molecule diffractive imaging in future XFEL experiments, provided that brilliance and pulse length allow this.

Acknowledgments

We thank Dr Ales Charvat for experimental help and advice concerning the microfluidic jet. The support of the Deutsche Forschungsgemeinschaft through SFB 755 Nanoscale Photonic Imaging and the Courant Research Centre Nano-Spectroscopy and X-Ray Imaging is acknowledged. The European Synchrotron Radiation Facility is acknowledged for providing excellent working conditions and beamtime.

References

[1] Gaffney K J and Chapman H N 2007 *Science* **316** 1444
[2] Neutze R *et al* 2000 *Nature* **406** 752
[3] Fienup J R 1982 *Appl. Opt.* **21** 2758
[4] Gerchberg R W and Saxton W O 1972 *Optik* **35** 237
[5] Miao J *et al* 2002 *Phys. Rev. Lett.* **89** 088303
[6] Marchesini S 2007 *Rev. Sci. Instrum.* **78** 011301
[7] Schroer C G *et al* 2008 *Phys. Rev. Lett.* **101** 090801
[8] Chapman H N *et al* 2006 *Nat. Phys.* **2** 839
[9] Huldt G, Szoke A and Hajdu J 2003 *J. Struct. Biol.* **144** 219
[10] Friedrich B and Herschbach D 1995 *Phys. Rev. Lett.* **74** 4623
[11] Stapelfeldt H 2004 *Phys. Scr.* T **110** 132
[12] Spence J H and Doak R B 2004 *Phys. Rev. Lett.* **92** 198102

[13] Starodub D *et al* 2005 *J. Chem. Phys.* **123** 244304
[14] Diat O, Roux D and Nallet F 1993 *J. Phys. II France* **3** 1427
[15] Wunenburger A S *et al* 2000 *Eur. Phys. J.* E **2** 277
[16] Sierro P and Roux D 1997 *Phys. Rev. Lett.* **78** 1496
[17] Safinya C R *et al* 1993 *Science* **261** 588
[18] Gulik-Krzywicki T *et al* 1996 *Langmuir* **12** 4668
[19] Pfohl T *et al* 2007 *Biomacromolecules* **8** 2167
[20] Jaspe J and Hagen S J 2006 *Biophys. J.* **91** 3415
[21] Charvat A *et al* 2004 *Rev. Sci. Instrum.* **75** 1209
[22] de Gennes P G and Prost J 1995 *The Physics of Liquid Crystals* (*International Series of Monographs on Physics* vol 83) (Singapore: World Scientific)
[23] Faubel M 1993 *Photoionization and Photodetachment* (*Advanced Series in Physical Chemistry* vol 10a) (Oxford: Oxford University Press)
[24] Zilman A G and Granek R 1996 *Phys. Rev. Lett.* **77** 4788
[25] Rheinstädter M, Häußler W and Salditt T 2006 *Phys. Rev. Lett.* **97** 048103
[26] Weierstall U *et al* 2008 *Exp. Fluids* **44** 675
[27] Katz E *et al* 2006 *J. Appl. Phys.* **100** 034313